

## ARTICLE

<https://doi.org/10.1038/s42005-020-0280-z>

OPEN

# Spin accumulation in photo-induced potential dimples generated in semiconductors

H. Sanada<sup>1\*</sup>, A.M. Stramma<sup>1</sup>, Y. Kunihashi<sup>1</sup>, Y. Tanaka<sup>1</sup>, H. Gotoh<sup>1</sup>, K. Onomitsu<sup>1</sup>, F. Tagarelli<sup>1</sup> <sup>1</sup>, M. Kohda<sup>2</sup>, J. Nitta<sup>2</sup> & T. Sogawa<sup>1</sup>

Conventional ways of confining charges in semiconductors employ advanced lithographic and crystal-growth techniques. The construction of micro/nano-scale structures is also essential for manipulating spins. However, existing techniques are not always flexible enough to control spins in appropriate positions and timings. Here we report an alternative mechanism, which enables us to design temporal and reconfigurable low-dimensional potentials. The formation of photo-induced potential dimples is deduced from time and spatially-resolved Kerr rotation measurements performed on a GaAs quantum well. Two-dimensional images of spin distributions reveal that the photo-injected electron spins in a small area illuminated by a pump light survive for a time that is two orders of magnitude longer than typical recombination lifetimes. The Kerr rotation dependence on the pump laser conditions implies that the temporally generated dimple-shaped potential profile induced by remote charges effectively confines the electrons and enhances the spin lifetime determined by fluctuating spin-orbit effective magnetic fields.

<sup>1</sup>NTT Basic Research Laboratories, NTT Corporation, 3-1 Morinosato-Wakamiya, Atsugi 243-0198, Japan. <sup>2</sup>Department of Materials Science, Tohoku University, 6-6-02 Aramaki-Aza Aoba, Aoba-ku, Sendai 980-8579, Japan. \*email: [haruki.sanada.xb@hco.ntt.co.jp](mailto:haruki.sanada.xb@hco.ntt.co.jp)

Designing potential profiles that confine charge carriers in a small region of semiconductor materials is the underlying basis of semiconductor devices and also of modern experiments performed during scientific research. Low-dimensional electron systems are also indispensable for exploring novel functionalities of semiconductor spintronics. The voltage control of spin-orbit interaction (SOI)<sup>1</sup> has been demonstrated by using electrons confined in an asymmetric quantum well (QW) structure. Unfortunately, the SOI also has an adverse effect on the spin coherence lifetime, which is shortened by the fluctuating spin-orbit magnetic fields associated with the random motion of the diffusive two-dimensional electrons<sup>2</sup>. The tunability of SOI provides a solution; a balanced Rashba<sup>3</sup> and Dresselhaus<sup>4</sup> SOI condition for two-dimensional electron gas (2DEG) in zinc-blende type semiconductors provides an SU(2) spin-rotation symmetry, and the resultant persistent spin helix mode can have an extended lifetime<sup>5–8</sup>. Another approach, which does not require the precise tuning of the Rashba SOI, is to reduce the confinement size; the spin relaxation mechanism can be suppressed by confining electrons spins further towards a one<sup>9–14</sup> or zero<sup>15–18</sup> dimensional area.

Until now, the conventional methods for realizing a low-dimensional confinement potential in semiconductors include a bottom-up approach based on self-assembled crystal growth<sup>19</sup>, and top-down fabrication techniques using lithography and etching for the precisely designed structures. However, the potential landscapes obtained by these methods restrict the carrier motion in predetermined areas or channels, which cannot be altered flexibly once their geometries are fixed. To incorporate the benefit of controllable SOI while preserving spin coherence, we require a more flexible potential that yields appropriate confinement at an appropriate timing.

Here, we report a way of realizing a reconfigurable confinement potential that is formed instantaneously by simple light exposure in a semiconductor thin layer. The feasibility of the light-induced

temporal confinement potential was revealed by time and spatially resolved Kerr rotation (KR) measurements of the spin dynamics in an undoped GaAs/AlAs QW. We found that the potential energy for the conduction band electrons was spatially modulated by charge carriers co-excited in a separate GaAs buffer layer. This fact enabled us to enhance the electron spin lifetime in the QW by reducing the spatial size of the photo-induced confinement. This temporal and reformable way of modulating potential profiles for spins in semiconductors offers a solution to extend the spin lifetime in a different approach from those reported previously<sup>5–18,20–27</sup>, and opens the way to the efficient control of spin coherence in future spintronics applications.

## Results

**Long-lasting Kerr signal from locally accumulated spins.** The KR measurements with well-focused pump and probe beams illuminated at a same position on the sample exhibited unexpectedly long-lasting spin signals. Figure 1a shows the layout for the pump and probe measurements. For time-resolved KR measurements in the absence of an external magnetic field, both the pump and probe wavelengths were tuned to the lowest heavy-hole exciton transition energy (1.530 eV). When we used a pump beam with a full-width-at-half-maximum (FWHM) diameter of 7.6  $\mu\text{m}$  (the red line in Fig. 1b), the KR angle ( $\theta_K$ ) survived even at  $\Delta t = 12$  ns, which is the maximum delay determined by the repetition interval of the mode-locked laser pulses. An exponential fit to the data for  $7 \text{ ns} \leq \Delta t \leq 12 \text{ ns}$  gives a time constant of 15.2 ns, which is two orders of magnitude longer than the typical radiative recombination lifetime (0.1–1 ns)<sup>28,29</sup>. The nonlinearity in the semi-log plot of KR at an earlier region of the delay time possibly originated from multiple causes including fast hole spin relaxation and diffusive dilution of spins in lateral directions. In the following discussion, we focus mainly on the slowly decaying exponential component observed in the KR data.

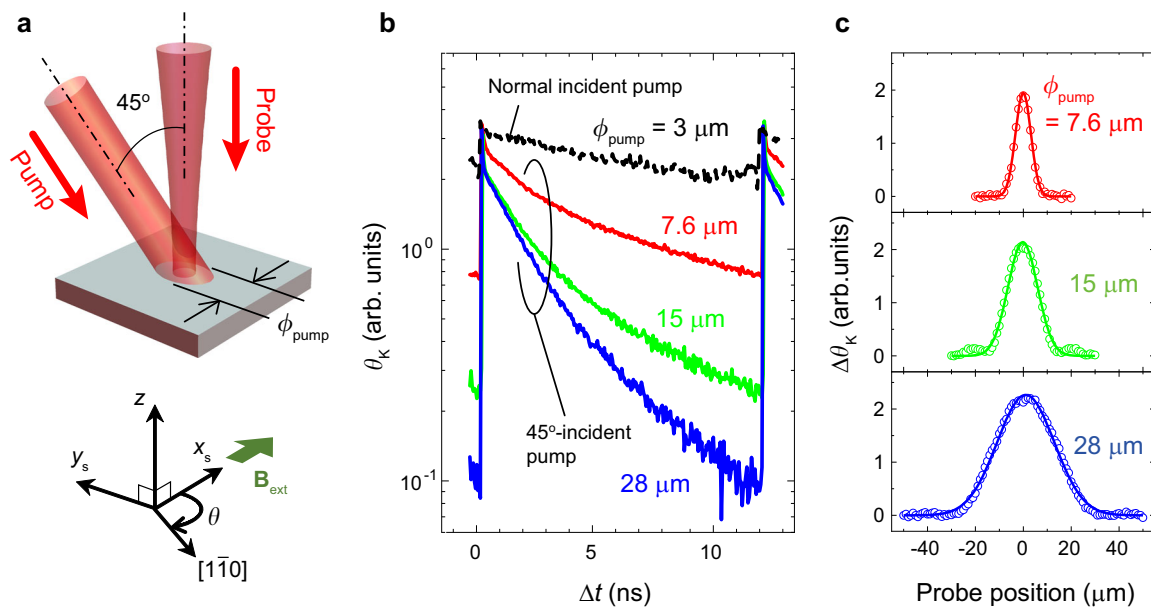


**Fig. 1 Time-resolved Kerr rotation measurement.** **a** Schematic view of the setup. **b** Kerr rotation angle ( $\theta_K$ ) as a function of pump and probe delay ( $\Delta t$ ) measured for different pump spot sizes in the absence of external magnetic field ( $\mathbf{B}_{\text{ext}}$ ). The vertical axis is plotted in a log-scale. The three solid lines show the data measured with a 45°-incident pump (setup shown in **a**), and their pump beam waist sizes ( $\phi_{\text{pump}}$ ) were characterized by the analysis of the data shown in **c**. The dashed line shows the data for a smaller pump spot ( $\phi_{\text{pump}} \sim 3 \mu\text{m}$ ) with a separate setup, which had collinear pump and probe beams along the sample normal. **c** The pump induced changes in the KR,  $\Delta\theta_K = \theta_K(\Delta t = +200 \text{ ps}) - \theta_K(\Delta t = -200 \text{ ps})$ , plotted as a function of the probe position scanned along the short axis of the elliptic pump spots. Fits to the data with the Gaussian (lines) give full-width at half maximum (FWHM) spot sizes of 7.6, 15, 28  $\mu\text{m}$ .

This long KR decay indicates that for some reason part of spin-polarized electrons or holes are accumulated in the illuminated area. Generally, in undoped semiconductors, a circularly-polarized light generates electron and holes, and thus both electron and hole dynamics or their recombination are expected to contribute to the spin dynamics of the whole system<sup>20–22</sup>. Because the KR decay time observed in our undoped QW was unexpectedly long, it requires an alternative explanation. A recently reported model for the long spin relaxation time observed in an undoped GaAs/AlGaAs interface<sup>23</sup> is not appropriate here because our sample has no single-hetero interface, where electron spins can be accumulated. Another possibility is isolated electrons resulting from dilute impurities unintentionally doped in the QW in the same way observed in *n*-doped GaAs<sup>24–26</sup>. However, we can exclude this possibility. The background impurity level of our GaAs epitaxial layer was estimated to be of the order of  $\sim 10^{14} \text{ cm}^{-3}$ , which corresponds to  $\sim 10^8 \text{ cm}^{-2}$  in the a 20-nm-thick QW, meaning that  $\sim 10^1$  spins trapped in the impurities must be detected with a 3- $\mu\text{m}$ -diameter probe. This number is too small for the KR signal detected in our measurements. In addition, our experimental results showing clear spin diffusion in the pumped area (discussed later) ruled out the possibility of a carrier trap caused by the impurities in the QW.

A striking feature of the KR signal was that its lifetime was clearly enhanced by reducing the size of the initial distribution of photo-injected spins. The set of data shown in Fig. 1b compares the dependence of the KR decay time on the pump spot size. The three solid lines were measured by changing the pump spot sizes with the measurement setup shown in Fig. 1a. The FWHMs of pump beam waists of 7.6, 15, and 28  $\mu\text{m}$  were obtained by fitting the pump induced changes in KR,  $\Delta\theta_K = \theta_K(\Delta t = +200 \text{ ps}) - \theta_K(\Delta t = -200 \text{ ps})$ , which were plotted as a function of the probe position along the short axis of the elliptic pump spot (Fig. 1c). The widths in the orthogonal direction were  $\sim 1.4$  times larger than these values, because the pump incident angle was inclined at  $45^\circ$  from the sample normal. To ensure that the pump power density at the center was the same for all the experimental conditions, we used a higher power for a pump focused on a larger spot size than for one focused on a smaller spot. As shown by the result in Fig. 1b, the KR decay time of the three data increases as the spot size decreases. We also measured the KR decay for a smaller pump spot size ( $\sim 3 \mu\text{m}$ ), which was achieved by focusing the pump through a higher magnification lens with a normal incident angle. Although the measurement condition was not completely the same as that of the setup with the  $45^\circ$ -incident pump, the KR result (dashed line) maintained the trend of KR lifetime enhancement and clearly shows the longest decay time among the four data. We note that a recent study<sup>27</sup> discusses the role of non-radiative excitons with large in-plane wave vectors as the source of the nanosecond spin lifetimes observed in an undoped QW. However, this possibility cannot fully explain the pump spot size dependence of the spin lifetime observed here.

**Spin diffusion in an excited area.** Evidence that electron spins diffuse in the pumped area was obtained by measuring the spatio-temporal behavior of spins in an externally applied magnetic field. To confirm the long-lived KR is determined solely by electrons, we employed the method reported by Kohda et al.<sup>30</sup>, which enables us to extract the momentum dependence of SOI. We defined the direction of  $\mathbf{B}_{\text{ext}}$  as the  $x_s$  axis and its perpendicular direction as the  $y_s$  axis. (see Fig. 1a). The application of  $\mathbf{B}_{\text{ext}}$  drives spin precession with an angular frequency  $\Omega = g\mu_B B_{\text{ext}}/\hbar$ , where  $g$  is the  $g$  factor,  $\hbar$  is the reduced Planck constant, and  $\mu_B$  is the Bohr magneton. The KR oscillations at the pump-probe overlap

( $x_s = 0$  and  $y_s = 0$ ) in Fig. 2a correspond to the spin precession determined solely by  $B_{\text{ext}} = 0.1 \text{ T}$  applied in the [100] direction. The extracted value,  $|g| = 0.32$ , is close to that of electrons observed in similar QW structures<sup>31</sup>. We did not see the beating of KR oscillation due to the coexistence of both electron and hole spins, indicating that hole spins are depolarized in a very short time. Then, motorized stages scanned the probe positions along the  $x_s$  axis and its perpendicular axis ( $y_s$ ). For both scanning directions, the KR signal did not show significant expansion in the QW plane in the measurement time range. When we scanned the probe position on the  $x_s$  ( $||[100]$ ) axis, the frequency  $\Omega$  changed monotonically at around the center; whereas it was almost constant for the scan along the  $y_s$  ( $||[010]$ ) direction. This phenomenon is discussed by Kohda et al.<sup>30</sup>; electrons at off-center positions have experienced non-zero averaged momentum, which induces additive or subtractive changes in the effective magnetic fields depending on the moving direction. Thus, the clear dependence of spin precessions on the probe position indicates that individual electron spins are not completely localized but move around in the excited area of the QW.

Further analysis of the spatially-dependent spin precession frequencies suggests the involvement of conduction band electrons as the source of the long-lived spins. As show in Fig. 2b, we extracted the spin-orbit-induced change in the spin precession,  $d\Omega/dx_s$  and  $d\Omega/dy_s$ , for different sample orientations defined by  $\theta$ , which is the angle of the in-plane crystallographic direction  $[1\bar{1}0]$  with respect to the  $x_s$  axis (see Fig. 1a). The sinusoidal dependences of  $d\Omega/dx_s$  and  $d\Omega/dy_s$  correspond to the vectors of the spin-orbit effective magnetic field plotted in a momentum space (Fig. 2c), which agrees with the symmetry of the  $k$ -linear Dresselhaus SOI for the conduction band but not for the valence band. Thus, from these results we infer that the conduction band electron spins contribute dominantly to the observed KR.

**Remote effect from charges excited in a separate layer.** Another important clue to the cause of the unexpectedly long-lasting KR was obtained from cw measurements of pump-induced reflectivity change ( $\Delta R$ ) and KR spectra, which indicated a contribution made by carrier excitation in a bulk GaAs buffer layer. Since spin-related signals are accumulated by a pump pulse train due to their long decay times (as discussed in Fig. 1b), we were able to observe clear pump-induced  $\Delta R$  and KR signals even when we used cw lasers rather than pulsed lasers. We fixed the cw probe energy ( $E_{\text{probe}}$ ) at around the HH exciton energy, and scanned the pump energy ( $E_{\text{pump}}$ ). As shown in Fig. 3, both  $\Delta R$  and KR have clear peak or dip structures at the HH exciton energy ( $E_{\text{pump}} = 1.530 \text{ eV}$ ) and the LH exciton energy ( $E_{\text{pump}} = 1.535 \text{ eV}$ ). The clear difference between the signs of the two KR features is because the electrons have opposite spin directions that are determined by the selection rule of the inter-band optical transition<sup>32</sup>. In addition to these reasonable spectrum shapes originating from the QW,  $\Delta R$  has notable features even at a lower pump energy ( $E_{\text{pump}} = 1.514 \text{ eV}$ ), which is around the free exciton or donor-bound exciton energies in bulk GaAs<sup>25</sup>. Such upconversion-like behavior in  $\Delta R$  was not observed in the KR spectrum, indicating that the pump at  $E_{\text{pump}} = 1.514 \text{ eV}$  does not excite spin polarized carriers in the QW. We infer that the electric field generated by the carriers excited in the bulk GaAs buffer layer remotely affects the electrons excited in the QW.

## Discussion

The experimental results described in Figs. 1, 2 indicate that the locally-generated spins do not expand, or expand only slightly, even though a clear signature of electron spin diffusion was observed in the spatially-resolved spin precession frequency. If we

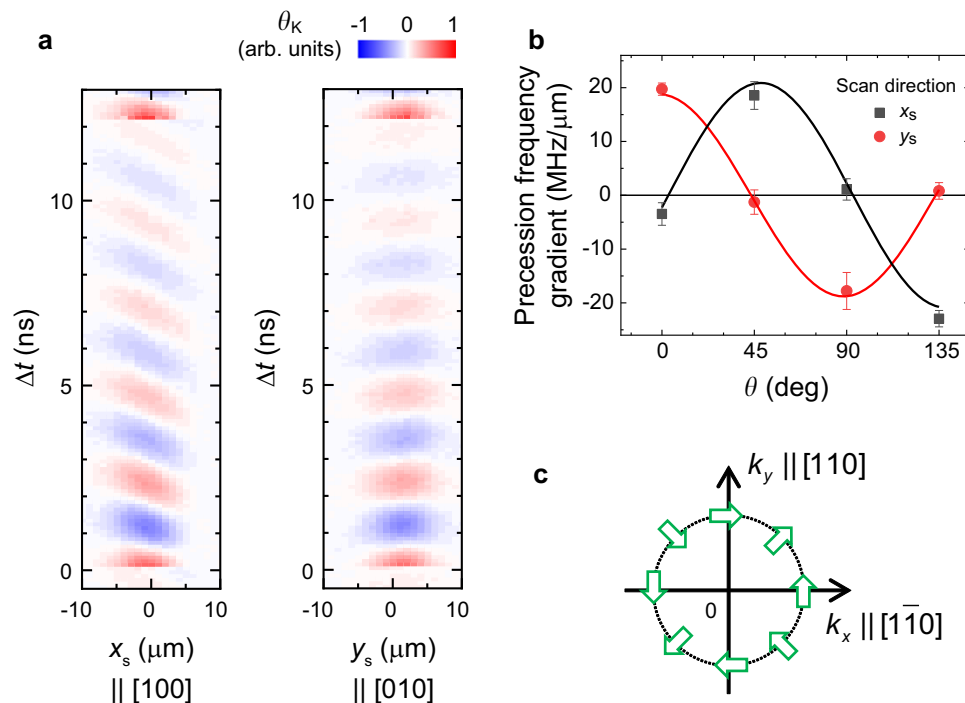


**Fig. 2 Spin diffusion dynamics measured under external magnetic fields.** **a** Density maps of Kerr rotation angle ( $\theta_K$ ) plotted as a function of the pump-probe delay ( $\Delta t$ ) and probe positions. We applied an external magnetic field ( $B_{\text{ext}} = 0.1\text{T}$ ) in the [100] direction and scanned the probe position in  $x_s$  ( $\parallel$ [100]) and  $y_s$  ( $\parallel$ [010]) axes. **b** The extracted spin precession frequency gradients in  $x_s$  (black squares) and  $y_s$  (red circles) directions are plotted as a function of  $\theta$ , which is the angle between the external magnetic field ( $\mathbf{B}_{\text{ext}}$ ) and the  $[\bar{1}\bar{1}0]$  direction. Error bars represent standard deviations resulting from the linear least-square fitting to the Kerr rotation oscillation frequencies. **c** The spin-orbit effective magnetic field vectors expected from the results shown in **b** are schematically plotted in momentum space.

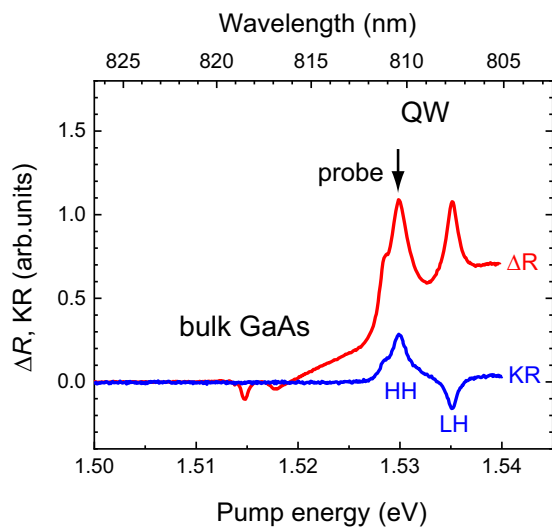


**Fig. 3 Pump energy dependence of optical reflectivity and Kerr rotation measured with a fixed probe energy.** Two-color measurements of the reflectivity change ( $\Delta R$ ) and Kerr rotation (KR) were performed with pump and probe beams from two identical continuous wave lasers. The probe energy (fixed at 1.530 eV) corresponds to the lowest electron-heavy hole exciton energy in the quantum well.

assume that 2DEG spins, or spins that diffuse over the region illuminated by the pump, are involved in the observed KR signal, the Gaussian spin density profile will initially expand with a speed determined by  $D_s$ . Because of this expansion, the upper limit of the KR decay constant at early times will be determined by a pre-factor<sup>33</sup>,  $\sigma_{\text{pump}}^2 / (\sigma_{\text{pump}}^2 + 2D_s t)$ , where  $\sigma_{\text{pump}} = \phi_{\text{pump}} / (2\sqrt{2 \ln 2})$ .

This diffusive dilution is more prominent for smaller  $\sigma_{\text{pump}}$  values. When we assume  $D_s = 25 \text{ cm}^2 \text{ s}^{-1}$  and  $\phi_{\text{pump}} = 3 \mu\text{m}$ , the diffusive dilution reduces the spin density by  $\sim 87\%$  of the initial value in 5 ns. However, we do not see such a rapid decay in the time-resolved data measured with a  $3 \mu\text{m}$  pump spot diameter (Fig. 1b). This fact suggests that the observed long-lasting KR was possibly assisted by additional forces that suppress the expansion of the locally generated electron spin density profile.

This characteristic behavior of the local spin distribution suggests the occurrence of the light-induced temporal confinement of electrons in the QW. As we have discussed in Fig. 3, the carriers excited in the bulk GaAs buffer layer should have a non-negligible electrostatic effect on the QW. Because carriers in the bulk GaAs buffer layer are co-excited even when we use the pump laser tuned at the QW energy, we can expect the similar remote effect also in the time-resolved measurements of spins in the QW (Figs. 1, 2). This is also supported by the fact that part of the carriers generated in the buffer layer persist over a timescale of  $\sim 10 \text{ ns}$  (Supplementary Note 1). In our study, the notable enhancement of the KR decay was observed when we shrank the pump spot sizes (3–28  $\mu\text{m}$ ) across the wavelength of the SOI-induced electron-spin precession ( $\lambda_{\text{SO}} \sim 24 \mu\text{m}$ )<sup>31,34</sup>. This fact implies that the observed spin dynamics are governed by the D'yakonov-Perel' spin relaxation mechanism<sup>8</sup> which can be suppressed by carrier confinement on the scale of the pump spot size. The temporal potential modulation in the QW can be induced by photo-generated space charges co-excited in the bulk GaAs buffer layer. Probable causes of these space charges are the dilute background impurities in the buffer layer. Because their positions are well separated from each other, electrons and holes trapped in these impurities cannot recombine in a short time. The resultant ionized impurities survive for a long time and affect the potential in the QW. Note that the dependence of KR on the

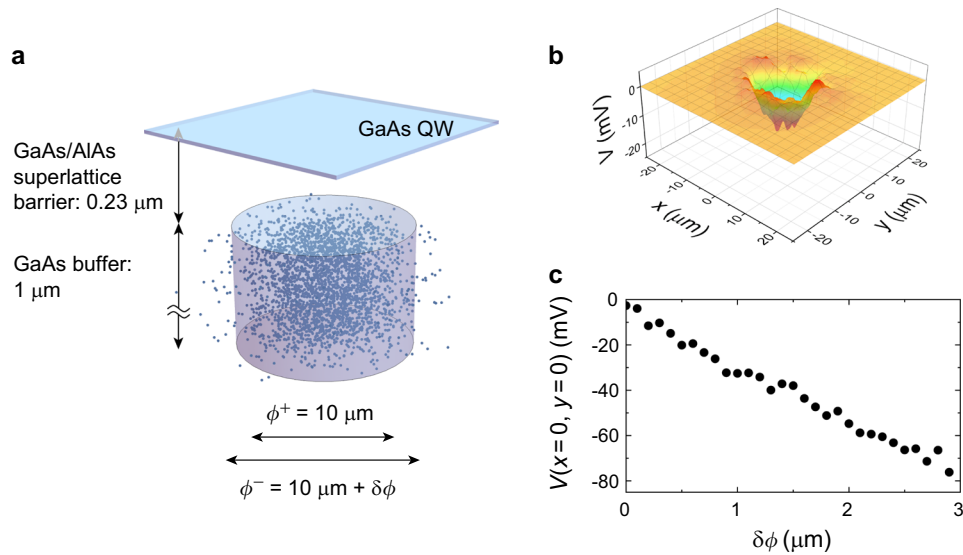


**Fig. 4** Calculation of the light induced confinement potential. **a** Schematic of the charge distribution assumed in the model. **b** Electro-static potential profile for electrons in the quantum well layer,  $V(x, y)$ , was calculated by assuming that the difference in distribution widths of positive and negative charges was  $\delta\phi = 0.5 \mu\text{m}$ . **c** The depth of the potential dimple ( $V$  at the position above the center of the charge distribution) as a function of  $\delta\phi$ .

bottom barrier thickness (Supplementary Note 2) and on the pump power (Supplementary Note 3) were also consistent with this assumption.

The above interpretation is also supported by our numerical simulations. Although it will require further careful study to identify the origin of the localized charge distributions that occur in the GaAs buffer layer, we can show that a small discrepancy in the negative and positive charge distributions induces a confinement potential with reasonable sizes and depths. Below we present a simple model that supports the possibility of photo-induced potential dimples that store electron spins in the separated QW layer.

We assume that the GaAs buffer layer has a small discrepancy in the charge expansions between positive and negative charge distributions, which can be caused by the different dynamics of electron and hole diffusion during their energy relaxation. To calculate the potential profile induced by these charges, we set the same number of positive and negative charges scattered randomly in the  $1 \mu\text{m}$  layer of GaAs with a uniform distribution in the  $z$ -direction, and a symmetric 2D normal distribution with FWHM widths of  $\phi^+ = 10 \mu\text{m}$ , and  $\phi^- = 10 + \delta\phi$  ( $\mu\text{m}$ ) for positive and negative charges, respectively (Fig. 4a). Figure 4b shows an example of the calculated potential in the QW layer, where we used  $10^{14} \text{cm}^{-3}$  for the positive charge concentrations at the center axis of doped area, and  $\delta\phi = 0.5 \mu\text{m}$ . The resultant bowl-shaped profile has a depth of  $\sim 20 \text{meV}$  and a size of  $\sim 10 \mu\text{m}$ . Figure 4c shows that the potential at the center becomes deeper as the  $\delta\phi$  value increases. These results indicate, if the deviation between the electron and hole distributions is of the order of  $0.1 \mu\text{m}$  or larger, the potential dimples induced by the dilute space charges are sufficiently effective to confine electrons at a low temperature.

To clarify the impact of light-induced confinement on the spin dynamics, we calculated the spatio-temporal evolution of photo-injected spins using a semi-classical Monte-Carlo approach (See Supplementary Note 4 for detailed procedure.). As a confinement potential generated by photo-generated remote charges, we assumed a simple two-dimensional parabolic function,

$$V(x, y) = C(x^2 + y^2), \quad (1)$$

where the prefactor  $C$  was chosen so that the potential maintains the lateral extent of the electron distribution at the initial

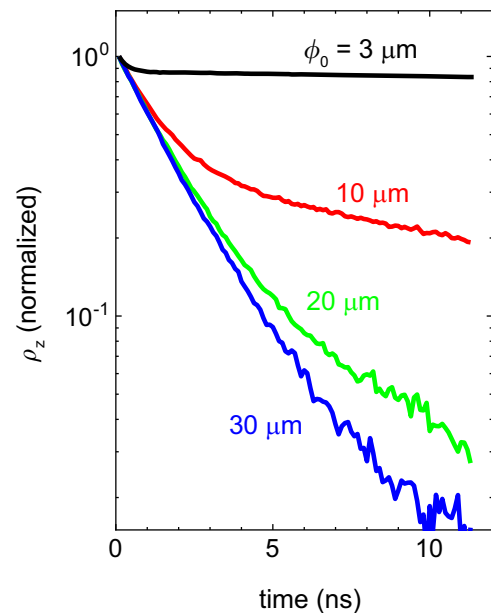


**Fig. 5** Monte-Carlo simulation of electron spins diffusing in a two-dimensional parabolic confinement potential. The  $z$ -components of spin density ( $\rho_z$ ) are plotted as a function of time for different initial Gaussian sizes ( $\phi_0$ ).

Gaussian shape determined by the pump spot sizes. The parameter used in the simulation was  $D_s = 25 \text{cm}^2 \text{s}^{-1}$ . For the spin-orbit interaction, we included only the  $k$ -linear Dresselhaus term with the strength  $\beta = 1.9 \text{meV}\text{\AA}$ , which should be dominant in the present system. For simplicity, we assumed a constant Fermi velocity  $v_F = 4.3 \times 10^4 \text{m s}^{-1}$  and ignored the dynamic change in the potential over time. The initial spin distributions were set as symmetric two-dimensional Gaussians with FWHM diameters of 3, 10, 20, and  $30 \mu\text{m}$ . Figure 5 shows the calculated spin density component along the  $z$ -axis as a function of delay time. As we expected, the calculated time scales of the spin decay clearly depend on the pump spot size. This agrees qualitatively with our results shown in Fig. 1b.

Thus, the motional narrowing effect for the spin dynamics determined by the D'yakonov-Perel' mechanism explains the observed phenomena quite reasonably.

In conclusion, a light-induced mesoscopic confinement potential significantly enhances electron spin lifetime in semiconductors. Such a temporal, non-destructive, and reconfigurable way of confining charges and spins is appealing for designing novel functionalities requiring the flexible motion of information carriers. The combination of this phenomenon with the current MEMS technology for scanning the light spot will also provide a possibility to change the potential with desired shapes and motions over time. Furthermore, the light-induced potential modulation can be effective for different materials or structures attached on the surface of semiconductors, since the electric field is remotely supplied from the space charges in a separate layer. The wavelength selectivity of the optical access for generating the space charges will allow us to scale up the desired temporal confinement areas towards multiple layers, indicating that the mechanism will be compatible with advanced band engineering. Thus, our photo-assisted method for confining electrons will provide fascinating options for exploring spin properties in semiconductors.

## Methods

**Sample.** The single QW was grown on a semi-insulating GaAs (001) substrate by molecular-beam epitaxy. The layer structure was, from the bottom, a 1- $\mu\text{m}$ -thick GaAs buffer, a 227-nm-thick short-period GaAs (1.4 nm)/AlAs (0.8 nm) superlattice bottom barrier, a 20-nm-thick GaAs QW, a 485-nm-thick top barrier, and a 5-nm-thick GaAs cap. All the layers were nominally undoped. The carbon impurity concentration in the epitaxial layer of nominally undoped GaAs was estimated to be of the order of  $10^{14} \text{ cm}^{-3}$  by SIMS measurements, and this agrees with the hole concentration obtained with conventional Hall measurements. The high crystal quality of the QW was expected from the fact that the 2DEG mobilities in high electron mobility transistor (HEMT) structures grown in the same MBE chamber were  $\sim 100 \text{ m}^2 \text{ V}^{-1} \text{ s}^{-1}$  at 4 K.

**Magneto-optic Kerr rotation measurements.** To investigate the dynamics of the local spin distribution, we carried out time and spatially resolved magneto-optic Kerr measurements at 8 K. A pair of mode-locked Ti:sapphire lasers provided 1.5 ps pump and 8 ps probe pulses at a frequency of 82 MHz for injecting and detecting spins in the QW. A photoelastic modulator (PEM) operating at 50.1 kHz modulated the pump beam polarization between left and right circular polarizations, and an acousto-optic modulator (AOM) operating at 52.0 kHz modulated the intensity of the linearly polarized probe beam. The difference between the modulation frequencies, 1.9 kHz, was used as the reference of lock-in detection. The circularly-polarized pump beam excited spin polarized electrons<sup>32,35</sup>, and subsequent spin density dynamics were measured through the magneto-optic Kerr effect of the reflected linearly polarized probe beam. The choice of the collimating and focusing lenses used for the pump beam allowed us to change the pump spot size. We consider that the circularly polarized pump both for  $0^\circ$  and  $45^\circ$  incident angles generates electron spins in the  $z$  direction, and the KR is proportional to the  $z$  component of spins in the QW. The  $\sim 3 \mu\text{m}$  (FWHM) spot of the probe beam can be scanned in the sample plane, which enabled us to measure two-dimensional images of the spin densities at a certain pump-probe delay time  $\Delta t$ . The optical powers for the pump and probe light were smaller than of the order of  $\sim \mu\text{W}$  and  $\sim 0.1 \mu\text{W}$ , respectively. We measured the output current of a balanced photodiode bridge through the lock-in amplifier and recorded it as the KR signal. In addition to KR, we also detected the reflected probe intensity  $R$  with a single photodiode. The small difference between  $R$  with and without pump excitation, i.e.,  $\Delta R = R_{\text{pump ON}} - R_{\text{pump OFF}}$ , was measured with a single photodiode in the same way as with the KR setup except that the pump was linearly polarized and its intensity was modulated with another AOM operating at 50.1 kHz instead of the PEM used in the KR measurements.

## Data availability

The datasets generated during and/or analysed during the current study are available from the corresponding author on reasonable request.

Received: 24 June 2019; Accepted: 23 December 2019;

Published online: 17 January 2020

## References

- Nitta, J., Akazaki, T., Takayanagi, H. & Enoki, T. Gate control of spin-orbit interaction in an inverted  $\text{In}_{0.53}\text{Ga}_{0.47}\text{As}/\text{In}_{0.52}\text{Al}_{0.48}\text{As}$  heterostructure. *Phys. Rev. Lett.* **78**, 1335–1338 (1997).
- D'yakonov, M. I. & Perel', V. I. Spin relaxation of conduction electrons in noncentrosymmetric semiconductors. *Sov. Phys. Solid State* **13**, 3023–3026 (1972).
- Bychkov, Y. & Rashba, E. I. Properties of a 2D electron gas with lifted spectral degeneracy. *JTEP* **39**, 66 (1984).
- Dresselhaus, G. Spin-orbit coupling effects in zinc blende structures. *Phys. Rev.* **100**, 580 (1955).
- Schliemann, J. & Loss, D. Anisotropic transport in a two-dimensional electron gas in the presence of spin-orbit coupling. *Phys. Rev. B* **68**, 165311 (2003).
- Bernevig, B. A., Orenstein, J. & Zhang, S.-C. Exact SU(2) symmetry and persistent spin helix in a spin-orbit coupled system. *Phys. Rev. Lett.* **97**, 236601 (2006).
- Koralek, J. D. et al. Emergence of the persistent spin helix in semiconductor quantum wells. *Nature* **458**, 610 (2009).
- Kunihashi, Y. et al. Drift transport of helical spin coherence with tailored spin-orbit interactions. *Nat. Commun.* **7**, 10722 (2016).
- Bournel, A., Dollfus, P., Bruno, P. & Hesto, P. Gate-induced spin precession in an  $\text{In}_{0.53}\text{Ga}_{0.47}\text{As}$  two dimensional electron gas. *Eur. Phys. J. Appl. Phys.* **4**, 1–4 (1998).
- Mal'shukov, A. G. & Chao, K. A. Waveguide diffusion modes and slowdown of D'yakonov-Perel' spin relaxation in narrow two-dimensional semiconductor channels. *Phys. Rev. B* **61**, R21413(R) (2000).
- Kiselev, A. A. & Kim, K. W. Progressive suppression of spin relaxation in two-dimensional channels of finite width. *Phys. Rev. B* **61**, 13115 (2000).
- Holleitner, A. W., Shi, V., Myers, R. C., Gossard, A. C. & Awschalom, D. D. Suppression of spin relaxation in submicron InGaAs wire. *Phys. Rev. Lett.* **97**, 036805 (2006).
- Kunihashi, Y., Kohda, M. & Nitta, J. Enhancement of spin lifetime in gate-fitted InGaAs narrow wires. *Phys. Rev. Lett.* **102**, 226601 (2009).
- Kunihashi, Y., Kohda, M. & Nitta, J. Semiclassical approach for spin dephasing in a quasi-one-dimensional channel. *Phys. Rev. B* **85**, 035321 (2012).
- Stotz, J. A. H., Hey, R., Santos, P. V. & Ploog, K. H. Coherent spin transport through dynamic quantum dots. *Nat. Mater.* **4**, 585–588 (2005).
- Berezovsky, J., Mikkelsen, M. H., Stoltz, N. G., Coldren, L. A. & Awschalom, D. D. Picosecond coherent optical manipulation of single electron spin in a quantum dot. *Science* **320**, 349–352 (2008).
- Press, D., Ladd, T. D., Zhang, B. & Yamamoto, Y. Complete quantum control of single quantum dot spin using ultrafast optical pulses. *Nature* **456**, 218–221 (2008).
- Markmann, S., Reichl, C. & Salis, G. Universal nuclear focusing of confined electron spins. *Nat. Commun.* **10**, 1097 (2019).
- Michler, P. (ed.) *Single Semiconductor Quantum Dots* (Springer, Berlin, 2009).
- Ostanický, T. et al. Electron- and hole-spin relaxation within excitons in GaAs quantum wells by non-degenerate pump-and-probe measurements. *Phys. Rev. B* **75**, 165311 (2007).
- Urdanivia, J. et al. Quenching of the exciton-spin relaxation via exchange interaction in GaAs/Al<sub>x</sub>Ga<sub>1-x</sub>As quantum wells. *Phys. Rev. B* **65**, 115336 (2002).
- Snoke, D. W., Rühle, W. W., Köhler, K. & Ploog, K. Spin flip of excitons in GaAs quantum wells. *Phys. Rev. B* **55**, 13789–13794 (1997).
- Nádovnik, L. et al. Long-range and high-speed electronic spin-transport at GaAs/AlGaAs semiconductor interface. *Sci. Rep.* **6**, 22901 (2016).
- Kikkawa, J. M. & Awschalom, D. D. Resonant spin amplification in n-type GaAs. *Phys. Rev. Lett.* **80**, 4313–4316 (1998).
- Dzhioev, R. I. et al. Low-temperature spin relaxation in n-type GaAs. *Phys. Rev. B* **66**, 245204 (2002).
- Fu, K.-M. et al. Millisecond spin-flip times of donor-bound electrons in GaAs. *Phys. Rev. B* **74**, 121304(R) (2006).
- Trifonov, A. V. et al. Nanosecond spin coherence time of nonradiative excitons in GaAs/AlGaAs quantum wells. *Phys. Rev. Lett.* **122**, 147401 (2019).
- Polland, H.-J., Schultheis, L., Kuhl, J., Göbel, E. O. & Tu, C. W. Lifetime enhancement of two-dimensional excitons by the quantum-confined stark effect. *Phys. Rev. Lett.* **55**, 2610–2613 (1985).
- Gurioli, M. et al. Temperature dependence of the radiative and nonradiative recombination time in GaAs/Al<sub>x</sub>Ga<sub>1-x</sub>As quantum-well structures. *Phys. Rev. B* **44**, 3115–3124 (1991).
- Kohda, M. et al. All-optical evaluation of spin-orbit interaction based on diffusive spin motion in a two-dimensional electron gas. *Appl. Phys. Lett.* **107**, 172402 (2015).
- Sanada, H. et al. Manipulation of mobile spin coherence using magnetic-field-free electron spin resonance. *Nat. Phys.* **9**, 280–283 (2013).
- Meier, F. & Zakharchenya, B. P. (eds) *Optical Orientation*. (Elsevier, Amsterdam, 1984).

33. Salis, G., Walser, M. P., Altmann, P., Reichl, C. & Wegscheider, W. Dynamics of a localized spin excitation close to the spin-helix regime. *Phys. Rev. B* **89**, 045304 (2014).
34. Sanada, H. et al. Acoustically induced spin-orbit interactions revealed by two-dimensional imaging of spin transport in GaAs. *Phys. Rev. Lett.* **106**, 216602 (2011).
35. Nastos, F. et al. Full band structure LDA and k-p calculations of optical spin injection. *Phys. Rev. B* **76**, 205113 (2007).

### Acknowledgements

We thank P.V. Santos for useful discussions. This work was supported by JSPS KAKENHI Grant Numbers JP15H05699 and JP16H03821.

### Author contributions

H.S., Y.K., H.G. and T.S. designed the experiments; K.O. and H.S. designed the sample structure; K.O. grew the sample; H.S., A.M.S. and F.T. performed the measurements; H.S. and Y.T. performed the numerical simulation; M.K. and J.N. provided theoretical support and conceptual advice; H.S. wrote the manuscript; and all the authors discussed the results and commented on the manuscript at all stages.

### Competing interests

The authors declare no competing interests.

### Additional information

**Supplementary information** is available for this paper at <https://doi.org/10.1038/s42005-020-0280-z>.

**Correspondence** and requests for materials should be addressed to H.S.

**Reprints and permission information** is available at <http://www.nature.com/reprints>

**Publisher's note** Springer Nature remains neutral with regard to jurisdictional claims in published maps and institutional affiliations.



**Open Access** This article is licensed under a Creative Commons Attribution 4.0 International License, which permits use, sharing, adaptation, distribution and reproduction in any medium or format, as long as you give appropriate credit to the original author(s) and the source, provide a link to the Creative Commons license, and indicate if changes were made. The images or other third party material in this article are included in the article's Creative Commons license, unless indicated otherwise in a credit line to the material. If material is not included in the article's Creative Commons license and your intended use is not permitted by statutory regulation or exceeds the permitted use, you will need to obtain permission directly from the copyright holder. To view a copy of this license, visit <http://creativecommons.org/licenses/by/4.0/>.

© The Author(s) 2020